Investigating microstructure of concentrated suspensions of anisotropic particles under shear by small angle neutron scattering

E. B. Mock and C. F. Zukoski[a)]

Department of Chemical and Biomolecular Engineering, University of Illinois, Urbana, Illinois 61801

(Received 10 November 2006; final revision received 18 February 2007)

Synopsis

The microstructure of dense suspensions of anisotropic particles that are ordered at rest is explored under shear as a function of particle anisotropy and shear rate using small angle neutron scattering. For suspensions containing spheres and mildly anisotropic heteronuclear dicolloids, after preshearing, long-range order is present in the form of randomly stacked hexagonally close packed layers. As the shear rate is increased, long-range directional order is lost. At even higher shear rates, long-range order is re-established in the form of hexagonally packed layers sliding over one another. Suspensions of ordered homonuclear dicolloids are polycrystalline at rest, and as the shear rate is increased, sliding hexagonally packed layers develop while at larger shear rates long-range order is lost. These results demonstrate surprisingly large effects of shear on the microstructures of suspensions containing particles with small changes in anisotropy. © *2007 The Society of Rheology.* [DOI: 10.1122/1.2716452]

I. INTRODUCTION

Hard and charge stabilized spheres in suspension show an order/disorder phase transition as volume fraction is raised, with the resulting crystals having equilibrium body centered cubic (BCC) or face centered cubic (FCC) structures, depending on the particle charge and ionic strength [Russel *et al.* (1989); Ramakrishnan and Zukoski (2004)]. Simulations and experimental results on molecular systems suggest that as the degree of anisotropy is raised, different crystalline microstructures are seen at the disorder/order phase boundary [Vega and Monson (1997); Bolhius and Frenkel (1997); Streib *et al.* (1962); Vegard (1932)]. For hard dumbbells (two spheres of diameter D with centers separated by distance L) and spherocylinders, with cylinders of length L and diameter D capped with spheres of diameter D, an isotropic/nematic phase transition is predicted to occur for $L/D > 3.7$. For $L/D < 0.35$, the first ordered phase is that of a plastic, or rotator, crystal, where there is center of mass ordering but no preferred direction of the director. Only as the volume fraction is raised above an L/D dependent volume fraction is a crystal with both positional and orientational order predicted to be the lowest free energy

a)Author to whom correspondence should be addressed; electronic mail: czukoski@uiuc.edu

microstructure. Experiments on N_2 demonstrate that the first crystalline phase of N_2 is that of a plastic crystal, while orientational order is achieved at higher particle densities [Mills *et al.* (1986)].

Supporting these predictions and molecular observations, recent studies by Mock (2006b) on suspensions of charge-stabilized anisotropic particles prepared by seeded emulsion polymerization with varying degrees of anisotropy found these particles to exhibit the predicted trends. The particles studied may be considered interpenetrating spheres of different diameters, d_1 and d_2. Here, when $d_2=0.52d_1$, the particles are referred to as heteronuclear dicolloids, while when $d_1=d_2$, the particles are referred to as homonuclear dicolloids. In this paper we explore the effects of shear on the microstructure of these suspensions with particular attention paid to shear induced positional and directional order/polycrystalline transitions.

Many studies of the effects of shear on the microstructure of ordered suspensions have focused on suspensions of uniform spheres [Chen *et al.* (1994a, 1994b, 1992); Chow and Zukoski (1995); Ackerson (1990); Loose and Ackerson (1994)]. Several studies have examined the mechanism of shear banding in suspensions of anisotropic cylindrical micelles and rod-like virus particles where, under shear, the particles separate into bands with unique microstructures [Fischer *et al.* (2002); Lopez-Gonzalez *et al.* (2004); Kang *et al.* (2006); Dhont *et al.* (2003)]. The role of anisotropy has been investigated in polydisperse suspensions to understand the influence of shear alignment in flow properties of gels consisting of anisotropic particles [Egres *et al.* (2005, 2006); Bergstrom (1996, 1998); Camerel *et al.* (2003); Ramsay and Lindner (1993)] showing that thickening is associated with hydrocluster formation and is most sensitive to the minor axis of the ellipsoidal particles.

Here, we investigate flow induced microstructures of suspensions of three particle types: spheres, heteronuclear dicolloids where $d_2=0.52d_1$, and homonuclear dicolloids where $d_1=d_2$. We report that the shear induced microstructures change as anisotropy is increased.

II. MATERIALS AND METHODS

A. Sample preparation

Charge stabilized polystyrene colloids of varying anisotropy and length scales less than 300 nm (Fig. 1) were prepared and dialyzed to equilibrium against 1×10^{-3} M KCl using the same procedures as described by Mock (2006a). Upon reaching equilibrium, the negatively charged latex suspensions were concentrated by dialyzing against a solution containing 1.1 weight percent PEG. Suspension volume fractions for concentrated particles were then determined by weight loss upon drying using a particle density of 1.05 g cm^{-3}. Using a solution of 1×10^{-3} M KCl, the samples were then diluted to a volume fraction of 0.42. Samples were also diluted to volume fractions of 0.01 so that single particle scattering could be obtained under static conditions to verify the particles were not aggregated, and in the form one would expect from SEM micrographs.

Zeta potentials of each sample were obtained using a Brookhaven Instruments Phase Analysis Light Scattering (ZetaPALS) device. For these measurements, the samples were diluted with a solution of 1×10^{-3} M potassium chloride in water to a particle concentration of 20 μg cm^{-3}. The samples were then filtered with syringe filters of 0.45 μm pore size (Corning Inc.) before performing the zeta potential measurements.

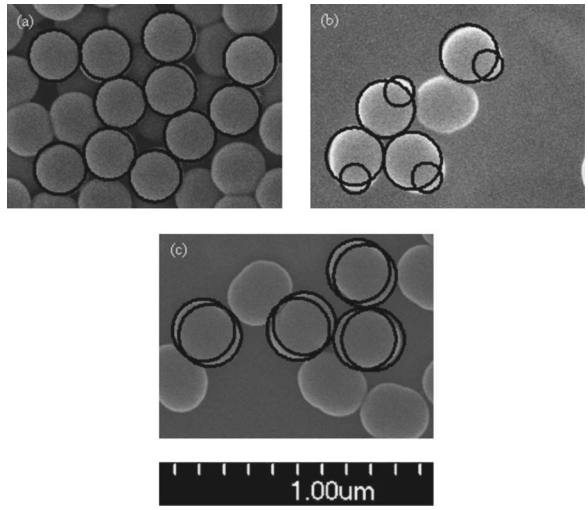

FIG. 1. SEM micrographs of the three classes of particles prepared: (a) spheres, (b) heteronuclear dicolloids, and (c) homonuclear dicolloids, along with overlapping particle models obtained with the Debye model for single particle scattering.

B. Rheological characterization

Flow properties of suspensions of spheres and homonuclear dicolloids at an ionic strength of 1×10^{-3}M and volume fraction of 0.42 were measured at 25 °C using a constant stress Bohlin CS-10 rheometer with a cup and bob geometry. The bob was roughened and had a diameter of 14 mm, and the inner diameter of the cup was 15.4 mm, yielding a gap size of 0.7 mm. Suspensions of spheres and homonuclear dicolloids were presheared at 100 and 50 s^{-1}, respectively, for 120 s and then allowed to rest for 1 h. Upon waiting 1 h after preshearing the samples, controlled rate experiments were performed with shear rate, $\dot{\gamma}$, between 0.15 and 15 s^{-1}. Steady-state stresses for spheres and homonuclear dicolloids were achieved in 720 and 900 s, respectively, and the integration time over which the shear rate was averaged was 30 s for both samples. For each suspension, shear rate was ramped up and then down, where data from both sweeps overlapped, illustrating the reproducibility of the data.

Oscillatory measurements were also performed where, after preshearing, the samples were allowed to rest for 10 s, so that the bob was allowed to reach a frequency of 1 Hz and shear stress, τ, of 0.14 Pa. Applying these values so as not to disrupt the suspension microstructure, the elastic modulus was measured as a function of time until it reached a constant, at which point it was assumed this constant value of elastic modulus, G_0, corresponded to that for the equilibrium microstructure of the particles in suspension.

C. Contrast variation

In the case of neutrons scattered from a suspension of particles, the scattering intensity, $I(q)$, may be expressed as

$$I(q) = \phi V_p (\Delta\rho)^2 P(q) S(q) + B, \tag{1}$$

where q is the wave vector, ϕ is the colloid volume fraction, V_p is the volume of a particle, $\Delta\rho$ is the difference between scattering densities of the solvent and colloid

particles, $P(q)$ is the form factor, $S(q)$ is the structure factor, and B is the background. The scattering densities may be calculated with

$$\rho = \frac{\sum b_i}{V}, \tag{2}$$

where Σb_i is the sum of the coherent scattering lengths of atoms and V is the volume occupied by these atoms [Stuhrmann (1982)]. Since neutrons scatter from nuclei, an element and an isotope of that element will have different scattering lengths. For example, hydrogen has a negative scattering length of -3.74×10^{-13} cm, while the scattering length of its deuterium isotope is 6.67×10^{-13} cm [Sears (1992)]. Thus, for neutron scattering, the scattering densities are found by

$$\rho = \frac{N_A \rho_m \sum b_i}{\sum m_{amu,i}}, \tag{3}$$

where N_A is Avogadro's Number, ρ_m is the density of the material, and $\Sigma m_{amu,i}$ is the sum of the atomic masses. Using a scattering length of 6.65×10^{-13} cm for carbon and 5.80×10^{-13} cm for oxygen, the neutron scattering densities for polystyrene and water are calculated as 1.41×10^{10} and -5.60×10^{9} cm^{-2}, respectively, and are sufficiently different that multiple scattering can be observed in dense suspensions [Cotton (1991)]. Contrast matching to reduce multiple scattering is achieved by using a mix of H_2O and D_2O (Aldrich, 99.9 atom % D).

For neutron scattering, it is possible to estimate the fraction of the beam that is scattered, f, using

$$f = 1 - \exp\left(-\frac{3}{2}\lambda^2 t \phi (\Delta\rho)^2 a\right) \tag{4}$$

where λ is the neutron beam wavelength, t is the sample thickness, $\Delta\rho$ is the difference in scattering densities between the particles and solvent, and a is the radius of the particles [Schelten and Schmatz (1980)]. Through a personal correspondence with Dr. John G. Barker at the National Institute of Standards and Technology Center for Neutron Research (NCNR) in Gaithersburg, MD, we learned that for a successful neutron scattering experiment, f should be between 0.002 and 0.2. For the small angle neutron scattering (SANS) experimental setup the neutron beam wavelength was 8 Å, sample thickness in the shear cell was 1 mm and, using a volume fraction of 0.42, to eliminate multiple scattering, a deuterium oxide to water ratio of 11:39 by mass would give an acceptable contrast difference. For a volume fraction 0.01, the suspensions were dilute enough that multiple scattering should not be present, even with no deuterium oxide added. Similarly, for ultra-small angle neutron scattering (USANS), where the neutron beam wavelength was 2.4 Å, it was found that deuterium oxide did not need to be added to prevent multiple scattering.

To ensure the correct $D_2O:H_2O$ ratio was maintained, the samples were concentrated by evaporation prior to adding D_2O. The correct mass of D_2O was added to reach the correct volume fraction and hold the ionic strength constant for all samples studied.

D. Small angle neutron scattering

SANS measurements were performed on the 30 m NG7 beamline at the NCNR under both static and shear conditions [Glinka *et al.* (1998)]. The instrument is equipped with a 640 mm × 640 mm 3He position-sensitive proportional counter 2D detector with a

5 mm × 5 mm resolution. The sample to detector distance used in this study was 15.3 m, and MgF_2 biconcave lenses were used to image the source aperture at the detector. Using cold neutrons with a wavelength of 8 Å and wavelength spread (full width at half maximum) of $\Delta\lambda/\lambda = 11\%$, trustworthy data was produced over a q-range of approximately 0.0015 to 0.01 $Å^{-1}$.

Suspensions at volume fractions of 0.42 were loaded into a Couette shear cell. The shear cell consists of an inner quartz cylinder with outer diameter 60 mm and an outer quartz cylinder of inner diameter 61 mm, such that the gap between the cup and bob was 0.5 mm. The inner quartz cylinder is static while the outer cylinder is rotated generating a Couette shear field between the cylinders, such that the flow direction is horizontal. The interior of the inner quartz bob is made of Invar, where the Invar material has a 0.75 in diameter hole in the center of the side facing the incoming beam and a larger hole on the opposite side. These holes accommodate an incident beam of diameter 0.5 in and the exiting scattered radiation.

Each sample was presheared at a shear rate of 1000 s^{-1} for 5 min and then left to rest for approximately 1 h in order for the equilibrium structure to build back in. The shear cell was mounted on a stage which also contained a single sample cell holder to perform static scattering with. Therefore, while the concentrated samples were waiting after preshear, the stage could be translated horizontally so that static scattering was performed on dilute samples in order to obtain single particle scattering. These dilute samples were loaded into demountable titanium cells with quartz windows. The demountable titanium cells have a path length of 1 mm and require a sample volume of 0.5 cm^3, and the exposed portion of the quartz windows have a diameter of about 0.75 in, such that they may accommodate an incident beam of 0.5 in diameter. The static scattering experiments lasted about 20 min, such that the counts on the detector were 2×10^5 or greater. Upon waiting for 1 h, scattering was performed from the concentrated suspensions in the Couette shear cell at rest and then at shear rates of 0.1, 0.175, 0.25, 0.325, 0.5, 0.625, 0.75, 1, 1.75, 2.5, 5, 10, and 100 s^{-1}. Each of these measurements was performed in the radial direction and lasted around 25 min in order to obtain 2×10^5 or more counts at the detector for every run.

As described earlier for the rheological characterization of flow properties, at shear rates of 0.15–15 s^{-1}, steady state stresses were achieved in 12–15 min, with stresses overlapping when the shear rate was ramped up and down. This suggests that performing SANS on these samples under shear for 25 min at each shear rate, the suspensions reached steady state approximately halfway through each run, if not earlier.

Scattering and transmission measurements were taken for the empty shear and static sample cells, and after these measurements were performed, the beam was blocked for each type of cell and scattering measurements performed in order to obtain the background scattering. The scattering measurements lasted 20 min and the transmission measurements were taken over a 3 min period. Transmission measurements were then taken from each of the concentrated and dilute samples for 3 min, so that the corrected sample data was obtained using

$$COR = (SAM - BGD) - \frac{T_{samp}}{T_{emp}}(EMP - BGD) \tag{5}$$

where COR, SAM, BGD, and EMP are the corrected, sample, background, and empty cell scattering data, respectively, and T_{samp} and T_{emp} are the transmission of the sample and empty cell, respectively.

E. Ultra-small angle neutron scattering

USANS measurements were performed on the perfect crystal diffractometer BT5 beamline at the Center for High Resolution Neutron Scattering (CHRNS) at the NCNR, under static conditions [Barker *et al.* (2005b)]. The instrument is of a Bonse-Hart nature, making use of channel-cut Si(220) crystals. A premonochromator made of pyrolytic graphite (002) diffracts the neutrons to the monochromator made of one of the Si(220) crystals prior to the sample, where the neutrons are reflected three times and the beam is directed to the sample. The beam is scattered towards the analyzer, made of the other Si(220) crystal, where it is again reflected three times, and by rotating the analyzer to a specific angle, only the neutrons scattered from the sample at that same angle are sent to the small angle scattering detector. By reflecting the neutrons three times in each of the crystals, a signal-to-noise ratio comparable to what would be obtained with a pinhole instrument is obtained.

With thermal neutrons at a wavelength of 2.4 Å and a wavelength spread (full width at half maximum) of $\Delta\lambda/\lambda=5.9\%$, the q-range investigated with this instrument was approximately 0.0001 to 0.002 $Å^{-1}$. Performing USANS under static conditions on dilute suspensions to obtain single particle scattering, this range of wave vectors overlaps with that obtained with SANS and so data from the two techniques may be combined to formulate a good picture of the single particle scattering from suspensions of spheres and anisotropic particles. Furthermore, the q-range obtained with USANS corresponds conveniently to the Guinier regime, and can be used to check for upturns signifying the presence of particle aggregates.

For the USANS experiments, the samples were loaded into the same demountable titanium cells with quartz windows, as for the static SANS experiments. A multiple position sample cell holder was used which could hold four sample cells at room temperature, such that it could be moved horizontally and continuous measurements could be performed on four samples. Besides the spheres, and heteronuclear and homonuclear dicolloids at volume fractions of 0.01, scattering was obtained from an empty sample cell in order to obtain corrected scattering data for the particles in water. Scans of each sample took approximately 6.5 h, while the blank took about 5.75 h.

III. RESULTS AND DISCUSSION

A. Scattering on static dilute suspensions

SANS and USANS were performed on dilute suspensions ($\phi=0.01$) of the particles shown in Fig. 1, to obtain single particle scattering over a wide range of wave vectors. Taking into account that for a sufficiently small volume fraction, $S(q)$ is unity for all q, then subtracting the background from the experimental single particle scattering intensity, $I_1(q)$, for spheres, it was fit with

$$\lim_{\phi\to 0} I_1(q) = \phi V_p(\Delta\rho)^2 P(q). \tag{6}$$

Assuming the anisotropic particles may be represented as two interpenetrating spheres, a seed sphere and a daughter sphere of equal or smaller size, single particle scattering from dilute suspensions of anisotropic particles was fit using the model of Debye (1915),

$$I_1(q) = \left(\frac{4\pi}{3}\rho\right)^2\left[a_s{}^6 P_s(q) + a_d{}^6 P_d(q) + 2a_s{}^3 a_d{}^3 (P_s(q)P_d(q))^{0.5}\frac{\sin(Lq)}{Lq}\right], \tag{7}$$

where a_s and a_d are the radii of the seed and daughter spheres, respectively, $P_s(q)$ and $P_d(q)$ are the form factors of the seed and daughter spheres, respectively, and L is the

TABLE I. Parameters used in model fits to single particle form factor scattering.

Sample	a (nm)	L (nm)	a_s (nm)	a_d (nm)	R_g (nm)
Spheres	105	–	–	–	81.3
Heteronuclear dicolloids	–	69	117	61	89.5
Homonuclear dicolloids	–	26	127	127	99.5

distance between the centers of the two spheres, as discussed previously by Mock (2006b). Since the polydispersity of the particles does not exceed the wavelength spread, it is acceptable to ignore any terms associated with polydispersity and, therefore, polydispersity is not accounted for in the previous models. The parameters used in these model fits are summarized in Table I. As seen in Fig. 2, the models fit the experimental data closely. Likewise, upon drawing model particles to scale using the parameters obtained from the model fits, and overlapping them with SEM micrographs of the particles, the resulting parameters appear to reasonably describe the spheres and anisotropic par-

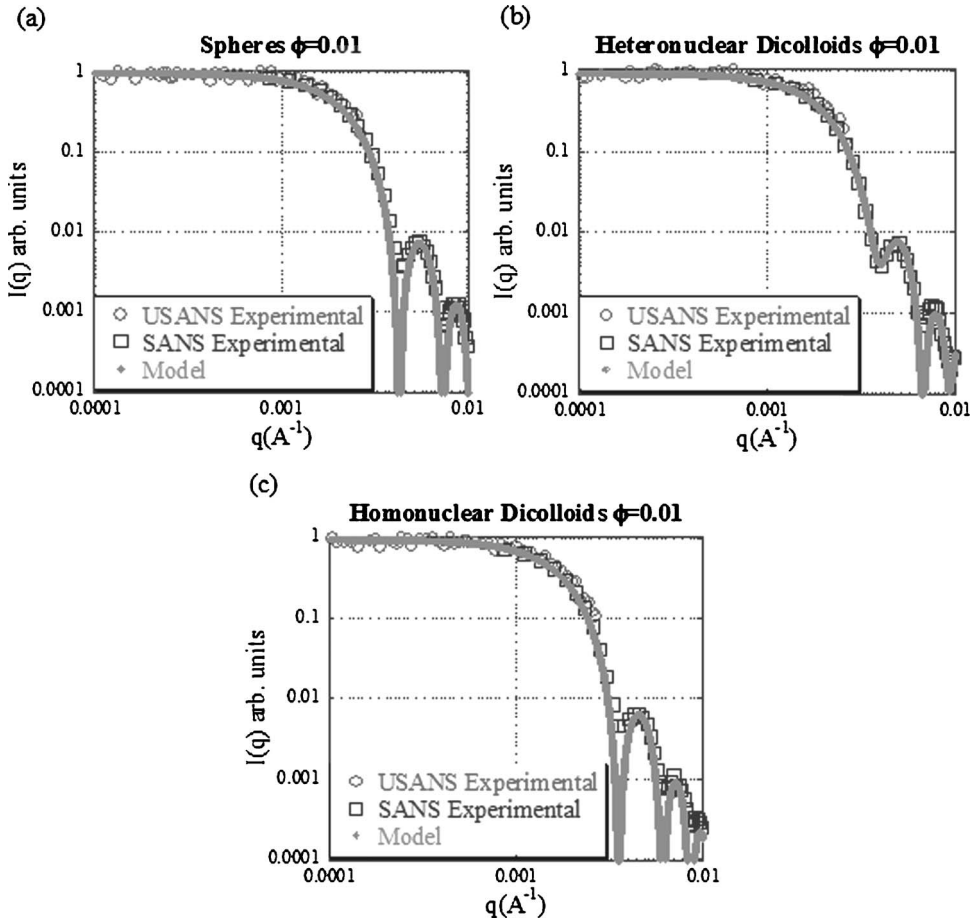

FIG. 2. Model fits to experimental single particle scattering data for the three classes of particles studied in this work: (a) spheres, (b) heteronuclear dicolloids, and (c) homonuclear dicolloids, where the scattering intensity has been normalized so that $\lim_{q\to 0} I(q)=1$.

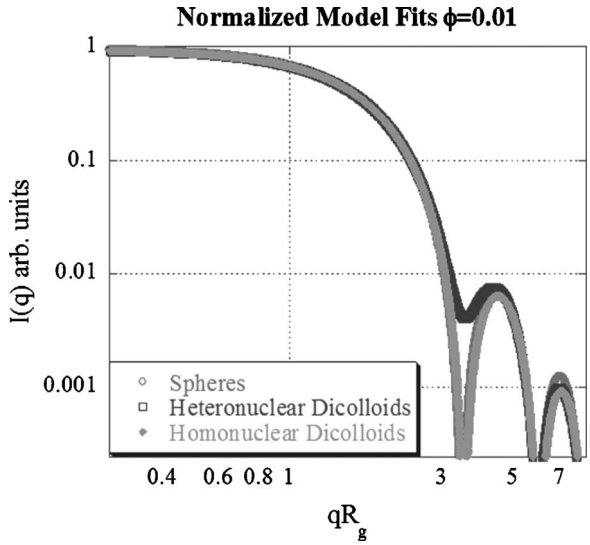

FIG. 3. Single particle scattering from spheres, and medium and homonuclear dicolloids, where the wave vector has been normalized by the radius of gyration, and the scattering intensity has been normalized so that $\lim_{q\to 0} I(q)=1$.

ticles (Fig. 1). That the Debye model fits the experimental data so closely may seem surprising since there is some overlap of the seed and daughter spheres, so that the scattering from this overlapped area is accounted for twice with Eq. (7). Part of the reason for this close fit to the experimental data may be that the particles are only weakly anisotropic, with $L/D<0.35$. However, there are still discrete differences between the scattering from the different types of particles in Fig. 2, which the model captures using the parameters in Table I, suggesting that Eq. (7) provides an estimate of the single anisotropic particle scattering. This agreement between the models and experimental data, especially in the small wave vector limit, suggests that the particles are not aggregated.

Combining SANS and USANS experiments, we see that both the plateau at small wave vectors and the maxima and minima at larger wave vectors are fit well by the models, thereby reaffirming our confidence in using them to describe single particle form factors. It is important to note that the USANS data is not desmeared, and both the SANS and USANS data are shifted in intensity to overlap and satisfy $\lim_{q\to 0} I(q)=1$ so that the intensity has arbitrary units. Upon calculating the radii of gyration, R_g, from model Guinier regimes, where $I_1(q)=(\Delta\rho)^2V_p^2\exp(-q^2R_g^2/3)$, and normalizing q by R_g on the x-axis, and the intensities such that $\lim_{q\to 0} I(q)=1$ (Fig. 3), the minima and maxima occur at the same values of qR_g for the spheres and anisotropic particles, as seen with ultra-small angle x-ray scattering (USAXS) in earlier work [Mock (2006b)]. Similarly, the maxima for the homonuclear dicolloids are slightly below the maxima for the spheres, which was also observed in previous studies [Mock (2006b); Johnson *et al.* (2005)].

B. SANS on concentrated suspensions under shear

SANS experiments were performed on concentrated suspensions ($\phi=0.42$) at rest and under shear. Figure 4 shows the 2D scattering pattern for planes of hexagonal close

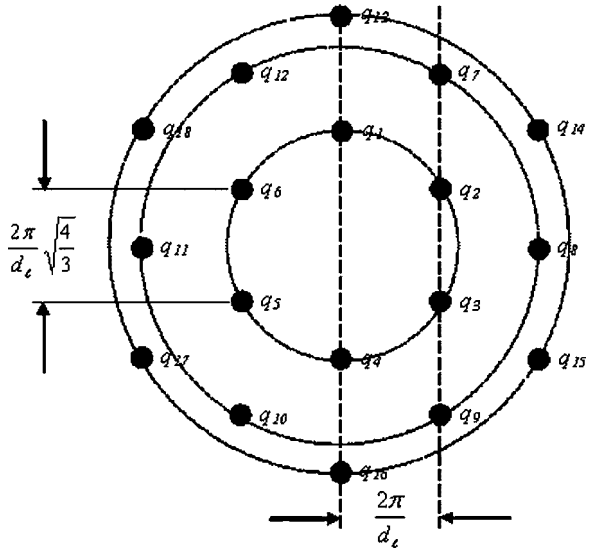

FIG. 4. 2D SANS pattern in q space for layers of hexagonal close packed spheres oriented normal to the incident neutron beam showing the intensity maxima in the first scattering rings.

packed spheres oriented normal to the incident neutron beam, where positions of maximum intensity are denoted as $q_1, q_2, \ldots$, and distances of separation between these high intensity spots are given based on the lattice parameter, d_ℓ. At rest, the suspensions of spherical particles were iridescent, indicating the particles were arranged in an ordered lattice, and SANS gave a 2D scattering pattern with six distinct intensity maxima in the inner ring, as well as a second ring with intensity maxima (Fig. 5) similar to that in Fig. 4. Detailed previous studies show that for radially directed, on-axis scattering, the six intensity maxima in the primary ring would not be present for a face centered cubic crystal (FCC), although the spots in both the primary and secondary rings would occur for a hexagonal close packed crystal (HCP) [Pusey and van Megen (1986); Loose and Ackerson (1994); Chen *et al.* (1994a, 1994b)]. After preshearing, the spheres are expected to be in layers with a random stacking sequence [Ackerson (1990); Versmold *et al.* (2002a)], and thus the microstructure at rest is best described as resulting from particles packed in randomly stacked HCP layers that are directionally ordered with an axis of closest packing along the velocity direction.

Applying a shear rate of 0.1 s^{-1}, the intensity maxima at positions q_1 and q_4 are weaker than the other four spots in the first scattering ring, where the ratio of the average of these two intensities to the average of the intensities at the other four spots is 0.69, implying that the crystal is strained [Chen *et al.* (1994a)]. Around 0.325 s^{-1}, the intensity maxima broaden, although the scattering rings are never completely uniform. These observations are consistent with previous studies on charge stabilized suspensions of ordered spheres [Vermant and Solomon (2005)] and indicate that at low shear rates, the scattering produces a powder pattern, indicating loss of long-range directional order. The primary scattering ring appears spotty at 1.75 s^{-1}, and by 5 s^{-1} the six intensity maxima are visible. At 100 s^{-1}, it is observed that the intensities of q_1 and q_4 are smaller than the other four spots in the first scattering ring, the ratio of the average of these two intensities to the average of the other four intensities being 0.49, suggesting that as the shear rate is increased above 0.325 s^{-1}, long-range directional order is re-established in the suspension

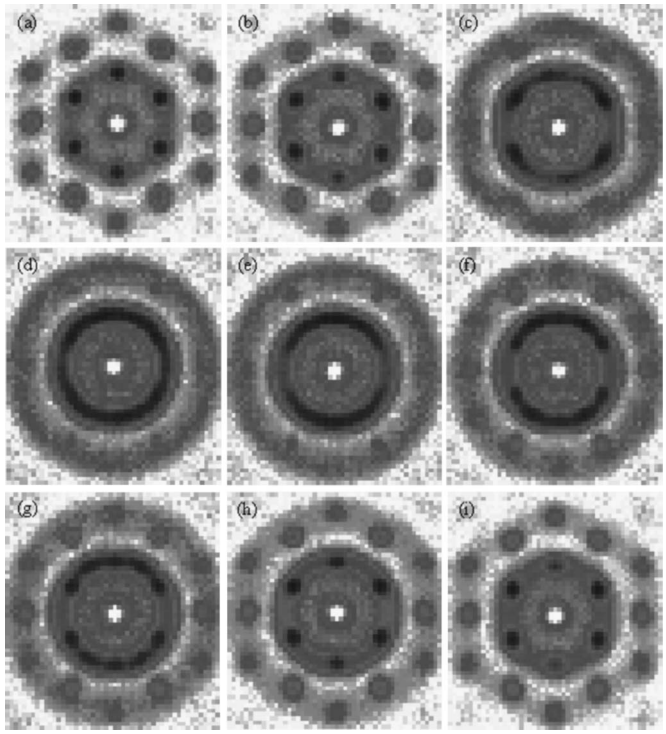

FIG. 5. 2D SANS plots, for spheres at various shear rates, (a) 0 s^{-1}, (b) 0.1 s^{-1}, (c) 0.175 s^{-1}, (d) 0.325 s^{-1}, (e) 0.625 s^{-1}, (f) 1.75 s^{-1}, (g) 2.5 s^{-1}, (h) 5 s^{-1}, and (i) 100 s^{-1}.

in the form of sliding layers of hexagonally packed spheres [Loose and Ackerson (1994); Chen *et al.* (1994a, 1994b); Ackerson (1990); Versmold *et al.* (2002b)].

To quantitatively explore how microstructure changes with shear rate, the intensities in the inner scattering ring of the 2D scattering patterns were measured. The change in the maximum and minimum intensities, I_{max} and I_{min}, were then investigated by plotting as a function of shear rate

$$I^* = \frac{I_{\max} - I_{\min}}{\langle I \rangle}, \tag{8}$$

where $\langle I \rangle$ is the average intensity in the primary scattering ring. For each shear rate, the intensities on the 2D scattering plots were averaged as a function of q in a sector, as illustrated in Fig. 6, where the central line in the figure was oriented at angles between 0° and 330° in increments of 30°. The two outside lines are the boundaries over which the data is averaged, and each is oriented at a specified angle about the central line. Then for each value of q along the central line, the intensity is averaged for all such values of q between the outer boundaries, and in this way a plot of averaged intensity as a function of q may be developed. In this study 15° for each of the two boundary lines was found to sufficiently capture each of the six primary intensity spots as well as each of the six areas between the primary intensity spots. The first peak in the sector averaged intensity versus q data corresponded to the intensity of the primary scattering ring captured by the sector, and maximum and minimum intensity of the twelve sectors were designated as I_{max} and I_{min}. The average intensity of the primary scattering ring, $\langle I \rangle$, was determined by

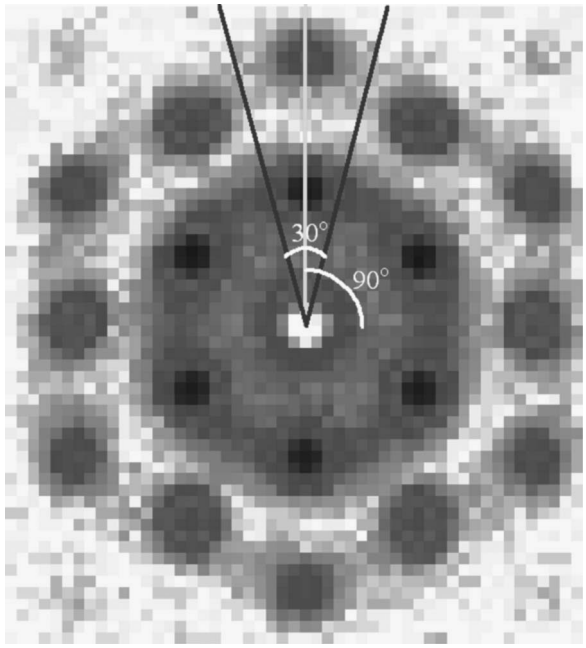

FIG. 6. Averaging intensity data over a sector oriented at 90° to the central q, and where the outer boundaries for the data collection are each oriented at 15° from the central line, such that the angle between them is 30°.

taking the average of the primary scattering ring intensities measured in this manner.

At rest, where the six intensity spots should be much greater in magnitude than the other regions of the scattering ring, the value of I^* will be relatively large. As shear broadens the intensity maxima, the intensity everywhere along the first scattering ring will be more similar and so I^* will decrease. However, as long-range order is reintroduced with even larger shear rates, I^* is expected to once again become larger.

At rest, $I^* = 2.0 \pm 0.2$, and applying shear drives this value down until eventually the directional order is completely destroyed around 0.325 s^{-1}, and I^* is only about 25% of its original value at rest (Fig. 7), indicating in a quantitative manner how the structure is broken up with increasing shear rate. Around 0.625 s^{-1}, the intensities in the region where q_1 and q_4 occur become larger, while intensities in other regions decrease, and as a result, I^* increases. Between 0.625 and 2.5 s^{-1}, I_{max} and I_{min} both decrease, and I^* is relatively constant at 0.84 ± 0.06. Finally, when distinct intensity spots appear above shear rates of 2.5 s^{-1}, I^* grows.

For spheres at rest, the lattice parameter, d_ℓ, was calculated by measuring the distance between q_5 and q_6 to obtain a value of 248 nm±5 nm. As a check and to make sure the second scattering ring had the same lattice parameter as the first, values of d_ℓ were also found using the distances between q_1 and q_6, q_{10} and q_4, and q_8 and q_3, which gave 254, 255, and 242 nm, respectively, yielding an average lattice parameter of 250±6 nm, where the uncertainty is well within the uncertainty of measuring the distances between the intensity maxima. To verify that the crystal structure was similar at 100 s^{-1} as at rest for spheres, the same four distances between intensity spots were measured to determine the lattice parameter. These four distances yielded an average lattice parameter of 253±2 nm.

At rest, the suspensions of heteronuclear dicolloids at a volume fraction of 0.42 give a scattering pattern similar to that obtained with spheres (Fig. 8), indicating a random

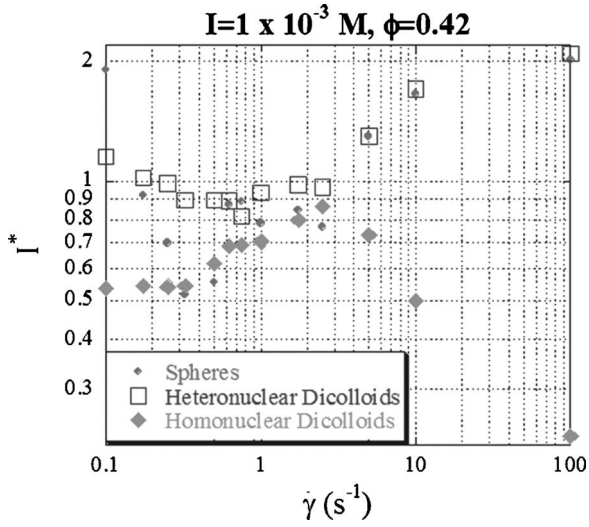

FIG. 7. I^* as a function of shear rate for spheres, heteronuclear dicolloids, and homonuclear dicolloids at a volume fraction of 0.42 and ionic strength of 1×10^{-3} M. At rest the value of I^* is, for spheres: 2.0±0.2, for heteronuclear dicolloids: 1.9±0.2, and for homonuclear dicolloids: 0.21±0.02.

stacking of HCP layers in agreement with results obtained using USAXS [Mock (2006b)]. When a small shear rate of 0.1 s^{-1} is applied to the suspension, long-range directional order is lost, although the scattering rings are not uniform, and so the sample

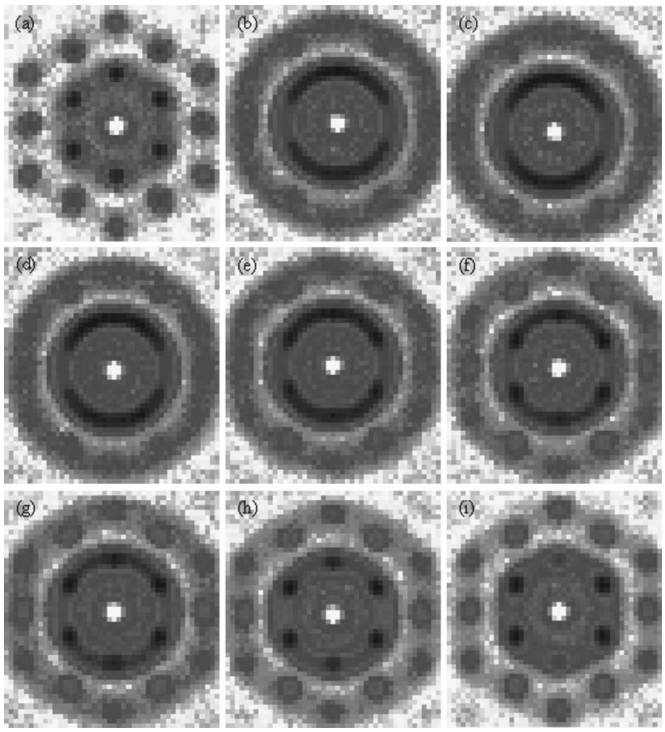

FIG. 8. 2D SANS plots, for heteronuclear dicolloids at various shear rates, (a) 0 s^{-1}, (b) 0.1 s^{-1}, (c) 0.175 s^{-1}, (d) 0.325 s^{-1}, (e) 1 s^{-1}, (f) 1.75 s^{-1}, (g) 2.5 s^{-1}, (h) 5 s^{-1}, and (i) 100 s^{-1}.

appears to be polycrystalline. This is in contrast to spherical particles which maintain long-range order in a strained crystal form at 0.1 s^{-1}. The different behavior for the heteronuclear dicolloids may indicate that the particle anisotropy results in crystals that are more easily degraded by shear.

For $\dot{\gamma} > 1$ s^{-1}, for the heteronuclear dicolloid sample, the primary scattering ring is spotty, and by 5 s^{-1}, the intensity maxima are visible. The behavior of heteronuclear dicolloids over these shear rates is thus very similar to that of spheres, and for both suspensions the onset of the phase transition from polycrystalline to directional order occurs at the same shear rates, indicated by the appearance of intensity maxima. As with suspensions of spheres, at 100 s^{-1} there are distinct intensity maxima in the first and second scattering rings, and the intensities at q_1 and q_4 are lower than the other four primary scattering ring spots, the ratio of the average of these intensities to the average of the other four intensities being 0.38, implying that at higher shear rates the heteronuclear dicolloids exist in the form of hexagonally packed layers sliding over one another.

At rest, for the plastic crystalline phase of heteronuclear dicolloids, I^* is 1.9 ± 0.2. Upon applying shear, long-range directional order is disrupted and I^* shrinks, as expected (Fig. 7). Between 0.325 and 2.5 s^{-1}, I_{max}, I_{min}, and $\langle I \rangle$ remain relatively constant, such that I^* is constant at 0.90 ± 0.09. As observed for spheres, when the primary scattering ring breaks up and distinct intensity spots appear above 2.5 s^{-1}, I^* increases.

The lattice parameters for the heteronuclear dicolloids at rest and under shear are calculated at shear rates of 0 and 100 s^{-1}. At rest, the average lattice parameter is 285 ± 2 nm while at 100 s^{-1}, the lattice parameter is 279 ± 6 nm. We expect the lattice parameter to scale approximately on the radius of gyration of the heteronuclear dicolloids. Thus, we find that $d_\ell / R_g = 3.2 \pm 0.3$ for the heteronuclear dicolloids and 3.1 ± 0.3 for the spheres indicating that within our ability to determine positions of intensity maxima, the heteronuclear dicolloids have structures very similar to the spheres at rest and under shear.

While suspensions of homonuclear dicolloids at a volume fraction of 0.42 were iridescent, 2D SANS patterns obtained gave primary and secondary scattering rings that were uniform with no evidence of spots of maxima intensity (Fig. 9). Although such a scattering pattern would suggest an amorphous structure, the iridescence of the suspension, as well as USAXS data reported by Mock (2006b) lead us to conclude that the 2D scattering data results from polycrystalline scattering. By a shear rate of 0.5 s^{-1}, the primary scattering ring becomes spotty, and the spots of maximum intensity gradually break in. For smaller shear rates, the suspensions of spheres and heteronuclear dicolloids lose directional order. Through shear rates of 1 to 2.5 s^{-1} intensity maxima in the primary and secondary scattering rings are clearly visible, and the intensity of the spots at q_1 and q_4 are slightly smaller than the four other spots in the first scattering ring, as the ratio of these two average intensities to the average intensities of the other four spots at 2.5 s^{-1} is 0.87. Rather than forming sliding layers at elevated shear rates above 2.5 s^{-1}, the spots of maximum intensity in the scattering rings broaden so that the suspensions appear to become polycrystalline. The homonuclear dicolloids thus display polycrystalline microstructures at low and high shear rates, but show greater directional order at intermediate shear rates.

Quantitatively investigating the flow properties of homonuclear dicolloids, in terms of I^*, at rest this value is found to be 0.21 ± 0.02. When shear rate is applied, the intensities at q_1 and q_4 increase in a manner similar to that of spheres after the long range order has been broken up, although as shear rate is increased through 0.325 s^{-1}, intensities in other regions of the primary scattering ring increase at the same rate as at q_1 and q_4, and I^* remains relatively constant (Fig. 7). Near a shear rate of 0.5 s^{-1}, where the primary

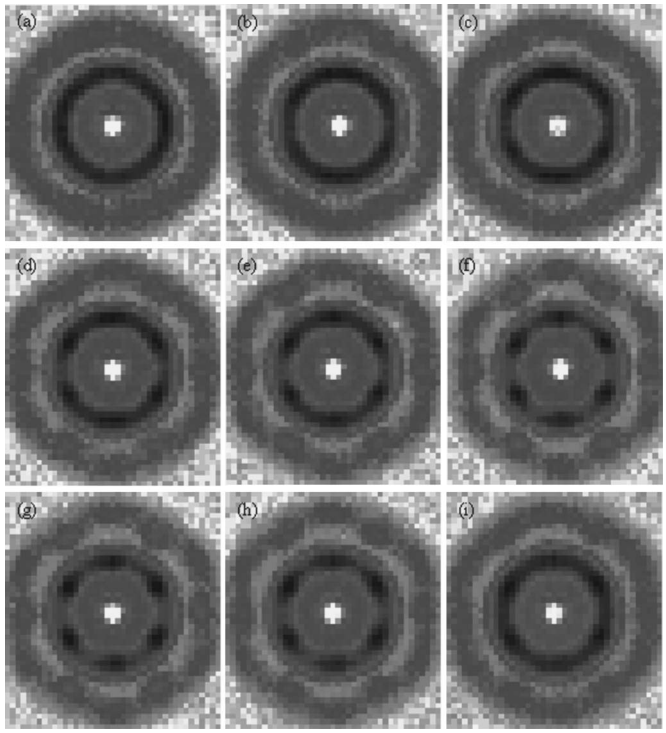

FIG. 9. 2D SANS plots, for homonuclear dicolloids at various shear rates, (a) 0 s^{-1}, (b) 0.325 s^{-1}, (c) 0.5 s^{-1}, (d) 0.75 s^{-1}, (e) 1 s^{-1}, (f) 1.75 s^{-1}, (g) 2.5 s^{-1}, (h) 5 s^{-1}, and (i) 10 s^{-1}.

scattering ring begins to break up into spots, I^* increases. As the intensity spots in the inner scattering ring become visible around 1 s^{-1}, I^* increases. As the intensity spots vanish above 2.5 s^{-1}, I^* decreases.

Since a scattering pattern with six primary intensity maxima is only obtained with homonuclear dicolloids under shear, lattice parameters were obtained at 2.5 s^{-1} using the same four distances between spots as with spheres, yielding an average lattice parameter of 297 ± 2 nm. Again, we find $d_\ell / R_g = 3.0 \pm 0.3$ indicating that the particles are packed into a lattice similar to that expected for spheres of similar size.

It is noteworthy that even when the homonuclear dicolloids are ordered, they appear to be less so than suspensions of spheres. One explanation for this may lie in the different particle zeta potentials determined by electrophoresis in an electrolyte with an ionic strength of 1×10^{-3} M. The spheres and heteronuclear dicolloids have zeta potentials of −16 and −11 mV, respectively while the homonuclear dicolloids were found to have a zeta potential of −0.35 mV. This decrease in magnitude of zeta potential with increasing degree of anisotropy is not surprising, as the swelling and secondary polymerization step used to obtain anisotropy increases the particle surface area while not adding any charge, thereby leading to a reduction of charge per particle surface area [Mock *et al.* (2006a)].

A second estimate of the surface potential can be made from the volume fraction where the particles order. If we assume effective hard interactions, both the spheres and the homonuclear dicolloids are expected to first show ordering at a volume fraction of 0.5 [Russel *et al.* (1989); Vega and Monson (1997)]. This suggests an effective sphere radius can be estimated from

$$\frac{\phi_{cryst}}{\phi_{eff}} = \frac{a^3}{a_{eff}{}^3}, \tag{9}$$

where ϕ_{cryst} is the volume fraction where ordering is first observed (0.28 for spheres and 0.37 for homonuclear dicolloids), ϕ_{eff}=0.5 is the volume fraction where hard spheres and spherocylinders of the same aspect ratio of the homonuclear dicolloids are expected to show order, a_{eff} is the effective hard sphere radius, and a is the particle radius. Calculating spherical sizes from the particle radius of gyration (Table I) through $R_g = \sqrt{\frac{3}{5}}a$, we find a=105 nm for the spheres and 128 nm for the homonuclear dicolloids. Following the treatment of Russel *et al.* (1989), the effective hard sphere size can be estimated by locating the particle separation when two particles interacting with electrostatic repulsions interact with a potential of kT. Using the linear superposition approximation, the pair potential for effective spheres with centers separated by more than $2a$, $\Phi(r)$, may be written

$$\frac{\Phi(r)}{kT} = \alpha \frac{\exp(-\kappa r)}{\kappa r}, \tag{10}$$

where k is Boltzmann's constant, r is the separation between particles, and α is

$$\alpha = 4\pi\varepsilon\varepsilon_0\psi_s^2 a^2 \kappa \frac{\exp(2a\kappa)}{kT}, \tag{11}$$

where ψ_s is the surface potential. The electric double layer length, κ^{-1}, may be determined by

$$\left(\frac{1}{\kappa}\right)^2 = \frac{\varepsilon\varepsilon_0 RT}{2IF^2}, \tag{12}$$

where ε is the dielectric constant, ε_0 is the permittivity of free space, R is the ideal gas constant, T is the temperature, I is the ionic strength, and F is Faraday's constant. Letting ε be the dielectric constant of water, then for a temperature of 25 °C and ionic strength of 1×10^{-3} M, κ^{-1}=10 nm. We seek the value of the surface potential when $\Phi(2a_{eff})/kT$=1. The surface potential values calculated in this manner for spheres and homonuclear dicolloids are 33 and 12 mV, respectively, again supporting the observation that the homonuclear dicolloids have a lower charge than the spheres.

At ϕ=0.42, both the spheres and homonuclear dicolloids are expected to be fully ordered [$\phi/\phi_{eff} > 1.1$, Russel *et al.* (1989)]. These calculations and observations indicate that while the homonuclear dicolloids are more weakly ordered, they are nevertheless fully ordered. The work of Chow and Zukoski (1995) explored the microstructural transitions when colloidal crystals are sheared. This work demonstrated that the polycrystalline to sliding layer structure was observed at $\phi/\phi_{cryst} \sim 1.05$ indicating that the effects of shear on microstructure seen in strongly ordered systems are preserved in weakly ordered systems.

X-ray scattering on similar samples at rest suggest that homonuclear dicolloids first order into a rotator, or plastic crystal, phase. The intensity maxima observed at intermediate deformation rates suggest that shear orients these crystals such that hexagonal layers are produced parallel to the walls of the rheometer and that these layers are destroyed at higher shear rates. We attribute this behavior to the particle shape. Further studies are required to confirm this conclusion.

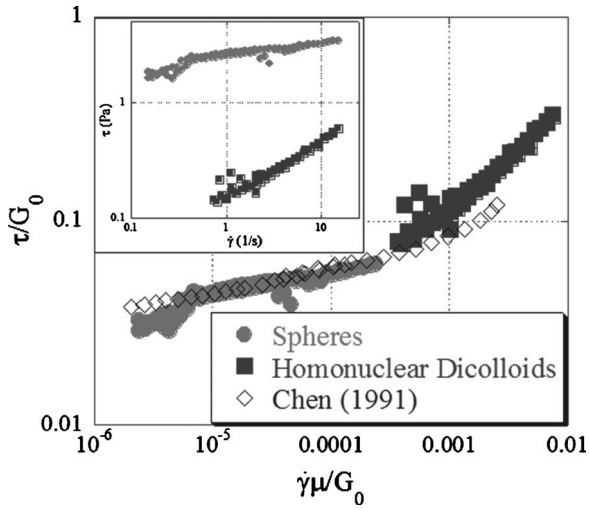

FIG. 10. Reduced shear stress as a function of reduced shear rate for spheres and homonuclear dicolloids at volume fraction of 0.42 and ionic strength of 1×10^{-3} M. The data of Chen (1991) is also plotted for negatively charged polystyrene spheres of diameter 229 nm and volume fraction 0.53 at ionic strength of 1×10^{-3} M.

C. Rheology on concentrated suspensions

Rheological measurements were performed on concentrated suspensions (ϕ=0.42) of spheres and homonuclear dicolloids. Plotting shear stress as a function of shear rate (Fig. 10), the values of shear stress are roughly an order of magnitude larger for spheres than homonuclear dicolloids, which in part may be attributable to the lower surface potential. Several studies have shown that the flow curves of suspensions composed of ordered spheres of different volume fractions, ionic strengths and sizes can be made to overlap when the stress is scaled on the elastic modulus of the suspensions, G_0, and the shear rate is scaled on G_0/μ, where μ is the viscosity of the continuous phase [Chow and Zukoski (1995); Fagan and Zukoski (1997)]. As shown in Fig. 10, the data sets from the spheres and homonuclear dicolloid suspensions do not overlap, but do seem to lie along a continuous curve. This belief is supported when compared with the reduced flow curve of Chen (1991) for negatively charged polystyrene spheres of diameter 229 nm and ϕ =0.53, suspended in an aqueous solution of 1×10^{-3} M KCl. The conversion of polycrystalline to sliding layer microstructures for the spheres in this study is completed near a shear rate of 8×10^{-5} G_0/μ. The observation of a shear induced six primary intensity maxima scattering pattern for the homonuclear dicolloids is seen near a shear rate of 1 $\times 10^{-3}$ G_0/μ, again emphasizing the different flow regime where long-range directional order is established in the homonuclear dicolloid suspension.

IV. CONCLUSIONS

The microstructure of anisotropic particles suspensions are examined under shear and compared to that of spheres using SANS and systematically changing anisotropy and shear rate. Concentrated suspensions are examined upon using dilute suspensions with USANS to determine that the particles are stable.

Single particle SANS and USANS data are found to be fit well by the Debye model, and the parameters obtained with this model sufficiently overlap with SEM images of the particles. Maxima and minima in the scattering curves of anisotropic particles and

spheres occur at the same values of qR_g, although there are small differences in the magnitude of intensity, particularly for the homonuclear dicolloids, which is in agreement with previous studies [Mock (2006b); Johnson *et al.* (2005)].

Concentrated suspensions of spheres and heteronuclear dicolloids are found to be ordered in hexagonal close packed arrangements at rest, and upon applying small shears, long-range order is still maintained, but the packing arrangement was strained. Eventually at moderate shears the long-range directional order is broken up and the suspension is polycrystalline. The heteronuclear dicolloids appear to have greater shear sensitivity and thus are driven to a polycrystalline state at a lower shear rate than the spheres. At large shear rates the suspension regains long-range order in the form of hexagonal layers sliding over one another. These results are consistent with those from studies on polystyrene spheres of similar sizes reported in previous literature [Chen *et al.* (1994a, 1994b; 1992)]. Furthermore, lattice parameters calculated from distances of separation between intensity spots in the 2D scattering plots seem to strengthen arguments that the spheres are in undistorted hexagonal arrangements.

Finally, SANS on concentrated, iridescent suspensions of homonuclear dicolloids at rest did not show evidence of long-range directional order. The presence of iridescence in these samples and USAXS scattering on similar samples provides evidence that these samples are ordered with layers of particles spaced at regular intervals (which gives rise to iridescence) with variable directional and orientational order within each layer. Increasing shear rate, long-range order develops, suggesting the presence of sliding hexagonal layers. For even larger shear rates, the long-range order is destroyed. Lattice parameters obtained from the 2D plots showing long-range order at moderate shear rates, suggest that the homonuclear dicolloids form undistorted hexagonal layers at these shear rates, which would be consistent with a plastic crystal phase. The differences in microstructure at rest and under shear between spheres and homonuclear dicolloids are particularly surprising since under static conditions USAXS experiments reported by Mock (2006b) suggest there is little difference in microstructure at these volume fractions. Rheological measurements of homonuclear dicolloids also show flow curves similar to those seen in suspensions of spheres but a wider volume fraction range must be probed to fully characterize the flow behavior.

For weakly anisotropic particles, of $L/D < 0.35$, in the plastic crystal phase, the results of this study imply that the suspensions under shear behave differently than spheres. In particular, as the anisotropy becomes sufficiently large, long-range order is introduced to the particle suspension as shear rate is increased, and is then lost at even larger shear rates. Over the same shear rates, for spheres, long-range order is broken up as shear rate is initially increased, and then reintroduced to the suspension at higher shear rates. These differences in suspension behavior under shear between spheres and anisotropic particles are intriguing, especially since the ordered structures obtained under both static conditions and shear appear to be very similar for spheres and the anisotropic particles investigated in this study.

ACKNOWLEDGMENTS

This work utilized facilities supported in part by the National Science Foundation under Agreement No. DIMR-0454672. We acknowledge the support of the National Institute of Standards and Technology, U.S. Department of Commerce, in providing the neutron research facilities used in this work. Research for this work was carried out in the Center for Microanalysis of Materials, University of Illinois, which is partially supported by the U.S. Department of Energy under grant DEFG02-91-ER45439. This material is

based upon work supported by the U.S. Department of Energy, Division of Materials Sciences under Award No. DEFG02-91ER45439, through the Frederick Seitz Materials Research Laboratory at the University of Illinois at Urbana-Champaign.

References

Ackerson, B. J., "Shear induced order and shear processing of model hard sphere suspensions," J. Rheol. **34**, 553–590 (1990).

Barker, J. G., C. J. Glinka, J. J. Moyer, M. H. Kim, A. R. Drews, and M. Agamalian, "Design and performance of a thermal-neutron double-crystal diffractometer for USANS at NIST," J. Appl. Crystallogr. **38**, 1004–1011 (2005b).

Bergstrom, L., "Rheological properties of Al_2O_3-SiC whisker composite suspensions," J. Mater. Sci. **31**, 5257–5270 (1996).

Bergstrom, L., "Shear thinning and shear thickening of concentrated ceramic suspensions," Colloids Surf., A **133**, 151–155 (1998).

Bolhius, P., and D. Frenkel, "Tracing the phase boundaries of hard spherocylinders," J. Chem. Phys. **106**, 666–687 (1997).

Camerel, F., J. C. P. Gabriel, P. Batail, P. Panine, and P. Davidson, "Combined SAXS-rheological studies of liquid-crystalline colloidal dispersions of mineral particles," Langmuir **19**, 10028–10035 (2003).

Chen, L. B., B. J. Ackerson, and C. F. Zukoski, "Rheological consequences of microstructural transitions in colloidal crystals," J. Rheol. **38**, 193–216 (1994a).

Chen, L. B., M. K. Chow, B. J. Ackerson, and C. F. Zukoski, "Rheological and microstructural transitions in colloidal crystals," Langmuir **10**, 2817–2829 (1994b).

Chen, L. B., C. F. Zukoski, B. J. Ackerson, H. J. M. Hanley, G. C. Straty, J. Barker, and C. J. Glinka, "Structural changes and orientational order in a sheared colloidal suspension," Phys. Rev. Lett. **69**, 688–691 (1992).

Chen, L. B., "The dynamic properties of concentrated charge stabilized suspensions," Ph.D. thesis, University of Illinois at Urbana-Champaign, Urbana-Champaign (1991).

Chow, M. K., and C. F. Zukoski, "Nonequilibrium behavior of dense suspensions of uniform particles: Volume fraction and size dependence of rheology and microstructure," J. Rheol. **39**, 33–59 (1995).

Cotton, J. P., "Initial Data Treatment," in *Neutron, X-Ray and Light Scattering: Introduction to an Investigative Tool for Colloidal and Polymeric Systems*, edited by P. Lindner and T. Zemb (North Holland, Amsterdam, 1991).

Debye, P., "Zerstreuung von Rontgenstrahlen," Ann. Phys. **351**, 809–823 (1915).

Dhont, J. K. G., M. Pavlik Lettinga, Z. Dogic, T. A. J. Lenstra, H. Wang, S. Rathgeber, P. Carletto, L. Willner, H. Frielinghaus, and P. Lindner, "Shear-banding and microstructure of colloids in shear flow," Faraday Discuss. **123**, 157–172 (2003).

Egres, R. G., and N. J. Wagner, "The rheology and microstructure of acicular precipitated calcium carbonate colloidal suspensions through the shear thickening transition," J. Rheol. **49**, 719–746 (2005).

Egres, R. G., F. Nettesheim, and N. J. Wagner, "Rheo-SANS investigation of acicular-precipitated calcium carbonate colloidal suspensions through the shear thickening transition," J. Rheol. **50**, 685–709 (2006).

Fagan, M. E., and C. F. Zukoski, "The rheology of charge stabilized suspensions," J. Rheol. **41**, 373–397 (1997).

Fischer, P., E. K. Wheeler, and G. G. Fuller, "Shear-banding structure oriented in the vorticity direction observed for equimolar micellar solution," Rheol. Acta **41**, 35–44 (2002).

Glinka, C. J., J. G. Barker, B. Hammouda, S. Krueger, J. J. Moyer, and W. J. Orts, "The 30 m small-angle neutron scattering instruments at the National Institute of Standards and Technology," J. Appl. Crystallogr. **31**, 430–445 (1998).

Johnson, P. M., C. M. van Kats, and A. van Blaaderen, "Synthesis of colloidal silica dumbbells," Langmuir **21**, 11510–11517 (2005).

Kang, K., M. P. Lettinga, Z. Dogic, and J. K. G. Dhont, "Vorticity banding in rodlike virus suspensions," Phys. Rev. E **74**, 026307 (2006).

Loose, W., and B. J. Ackerson, "Model calculations from the analysis of scattering data from layered structures," J. Chem. Phys. **101**, 7211–7220 (1994).

Lopez-Gonzalez, M. R., W. M. Holmes, P. T. Callaghan, and P. J. Photinos, "Shear banding fluctuations and nematic order in wormlike micelles," Phys. Rev. Lett. **93**, 268302 (2004).

Mills, R. L., B. Olinger, and D. T. Cromer, "Structures and phase diagrams of N_2 and CO to 13 GPa by x-ray diffraction," J. Chem. Phys. **84**, 2837–2845 (1986).

Mock, E. B., H. De Bruyn, B. S. Hawkett, R. G. Gilbert, and C. F. Zukoski, "Synthesis of anisotropic nanoparticles by seeded emulsion polymerization," Langmuir **22**, 4037–4043 (2006a).

Mock, E. B., "Synthesis, microstructure, and mechanics of charge stabilized anisotropic nanoparticles," M.S. Thesis, University of Illinois at Urbana-Champaign, Urbana-Champaign (2006b).

Pusey, P. N., W. van Megen, P. Bartlett, B. J. Ackerson, J. G. Rarity, and S. M. Underwood, "Structure of crystals of hard colloidal spheres," Phys. Rev. Lett. **63**, 2753–2756 (1989).

Ramakrishnan, S., and C. F. Zukoski, "Phase behavior of nanoparticle suspensions," in *Dekker Encyclopedia of Nanoscience and Nanotechnology*, edited by J. A. Schwartz, C. I. Contescu, and K. Putyera (Marcel Dekker, New York, 2004).

Ramsay, J. D. F., and P. Lindner, "Small-angle neutron scattering investigations of the structure of thixotropic dispersions of smectite clay colloids," J. Chem. Soc., Faraday Trans. **89**, 4207–4214 (1993).

Russel, W. B., D. A. Saville, and W. R. Schowalter, *Colloidal Dispersions* (Cambridge University Press, Cambridge, 1989).

Schelten, J., and W. Schmatz, "Multiple-scattering treatment for small-angle scattering problems," J. Appl. Crystallogr. **13**, 385–390 (1980).

Sears, V. F., "Neutron scattering lengths and cross sections," Neutron News **3**, 26–37 (1992).

Streib, W. E., T. H. Jordan, and W. N. Lipscomb, "Single-crystal x-ray diffraction study of β nitrogen," J. Chem. Phys. **37**, 2962–2965 (1962).

Stuhrmann, H. B., "Contrast variation," in *Small angle X-ray scattering*, edited by O. Glatter and O. Kratky (Academic Press, London, 1982).

Vega, C., and P. A. Monson, "Plastic crystal phases of hard dumbbells and hard spherocylinders," J. Chem. Phys. **107**, 2696–2697 (1997).

Vegard, L., "Structure of nitrogen and the different phosphorescence of the two forms of solid nitrogen," Z. Phys. **79**, 471–491 (1932).

Vermant, J., and M. J. Solomon, "Flow-induced structure in colloidal suspensions," J. Phys.: Condens. Matter **17**, R187–R216 (2005).

Versmold, H., S. Musa, and A. Bierbaum, "Concentrated colloidal dispersions: On the relation of rheology with small angle x-ray and neutron scattering," J. Chem. Phys. **116**, 2658–2662 (2002a).

Versmold, H., Ch. Dux, and S. Musa, "On the structure of charge stabilized polymer dispersions," J. Mol. Liq. **98-99**, 145–162 (2002b).